Conformational Substates of Calmodulin Revealed by Single-Pair Fluorescence Resonance Energy Transfer: Influence of Solution Conditions and Oxidative Modification†

Brian D. Slaughter,‡ Jay R. Unruh,‡ Michael W. Allen,‡ Ramona J. Bieber Urbauer,§ and Carey K. Johnson*,‡

Department of Chemistry, 1251 Wescoe Hall Drive, University of Kansas, Lawrence, Kansas 66045-7582, and Department of Chemistry and Department of Biochemistry and Molecular Biology, University of Georgia, Athens, Georgia 30602

Received July 2, 2004; Revised Manuscript Received October 26, 2004

ABSTRACT: A calmodulin (CaM) mutant (T34,110C-CaM) doubly labeled with fluorescence probes AlexaFluor 488 and Texas Red in opposing domains (CaM-DA) has been used to examine conformational heterogeneity in CaM by single-pair fluorescence resonance energy transfer (spFRET). Burst-integrated FRET efficiencies of freely diffusing CaM-DA single molecules yielded distributions of distance between domains of CaM-DA. We recently reported distinct conformational substates of Ca^{2+}-CaM-DA and apoCaM-DA, with peaks in the distance distributions centered at ∼28 Å, 34−38 Å, and 55 Å [Slaughter et al. (2004) *J. Phys. Chem. B 108,* 10388−10397]. In the present study, shifts in the amplitudes and center distances of the conformational substates were detected with variation in solution conditions. The amplitude of an extended conformation was observed to change as a function of Ca^{2+} over a free Ca^{2+} range that is consistent with binding to the high affinity, C-terminal Ca^{2+} binding sites, suggesting the existence of communication between lobes of CaM. Lowering pH shifted the relative amplitudes of the conformations, with a marked increase in the presence of the compact conformations and an almost complete absence of the extended conformation. In addition, the single-molecule distance distribution of apoCaM-DA at reduced ionic strength was shifted to longer distance and showed evidence of an increase in conformational heterogeneity relative to apoCaM-DA at physiological ionic strength. Oxidation of methionine residues in CaM-DA produced a substantial increase in the amplitude of the extended conformation relative to the more compact conformation. The results are considered in light of a hypothesis that suggests that electrostatic interactions between charged amino acid side chains play an important role in determining the most stable CaM conformation under varying solution conditions.

Calmodulin (CaM)[1] is a small (148 residues), Ca^{2+}-signaling protein that is involved in intricate and interrelated cellular processes, including smooth muscle contraction and Ca^{2+} homeostasis (*1, 2*). Increases in cellular Ca^{2+} levels lead to Ca^{2+} activation of CaM, which induces structural changes that expose hydrophobic patches that enable CaM to recognize a wide variety of targets (*3, 4*). There are four Ca^{2+} binding sites, two in each globular domain. It is well established that the C-terminal domain of CaM (sites III and IV) binds Ca^{2+} with about an order of magnitude higher affinity than the N-domain (sites I and II) (*5*−*7*). A structure of Ca^{2+}-CaM (pdb 1cll) (*8*) is shown in Figure 1A, with calcium binding sites I through IV labeled, as well as the sites of attachment of fluorescent probes Alexa Fluor 488 (AF488) and Texas Red (TR). A recent single-pair fluorescence resonance energy transfer (spFRET) study in our laboratory revealed the existence of multiple, distinct conformations of CaM-DA that persist out to the millisecond time scale (*9*). In the current study, distributions of CaM-DA were obtained under a variety of solution conditions to investigate the nature of CaM conformations in solution.

The observation of changes in CaM upon Ca^{2+} activation (*8, 10*−*13*) has raised important questions regarding the structural and dynamic origins of CaM's ability to activate diverse targets, some of which have little sequence homology. The majority of CaM targets contain two, separated hydrophobic areas. As the exposed hydrophobic patches of Ca^{2+}-CaM recognize the target, Ca^{2+}-CaM engulfs the target to shield these hydrophobic areas, bringing the N-terminal and C-terminal lobes of CaM into close proximity. Electrostatics plays a role in the relative orientation of CaM and its target, with negatively charged side chains in CaM being attracted to positively charged residues in many of the targets (*4*). The central linker between domains of CaM is highly

† This research was supported by NIH Grant ROI GM58715. B.D.S. and J.R.U. acknowledge support from the Dynamic Aspects of Chemical Biology NIH training grant (NIH 5 T32 GM08545-09).

* Corresponding author. E-mail: ckjohnson@ku.edu. Tel: (785) 864-4219. Fax: (785) 864-5396.

‡ University of Kansas.

§ University of Georgia.

[1] Abbreviations: CaM, calmodulin; AF488, Alexa Fluor 488 maleimide; TR, Texas Red maleimide; CaM-DA, a CaM mutant with cysteine substituted at sites 34 and 110 and doubly labeled with AF488 and TR; spFRET, single-pair fluorescence resonance energy transfer; EGTA, ethylene glycol-bis(2-aminoethylether)-*N*,*N*,*N*′,*N*′-tetraacetic acid; HEPES, *N*-(2-hydroxyethyl)piperazine-*N*′-(4-butanesulfonic acid); PMCA, plasma-membrane Ca^{2+}-ATPase; TCSPC, time-correlated single photon counting; 5,5′-dibromo-BABTA, 1,2-bis(2-amino-5-bromophenoxy)ethane-*N*,*N*,*N*′,*N*′-tetraacetic acid.

10.1021/bi048595o CCC: $30.25
Published on Web 02/11/2005

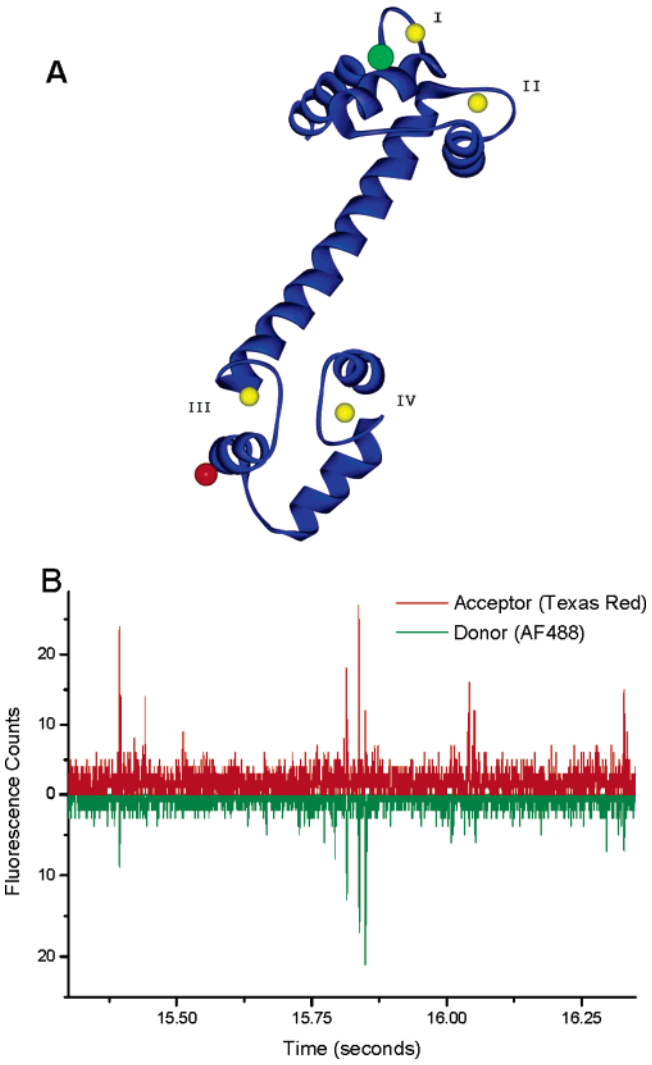

FIGURE 1: (A) Structure of Ca^{2+}-CaM (pdb 1cll (*8*)). Red and green spheres represent the sites of attachment of probes Texas Red and AF488. Calcium binding sites I through IV are labeled. (B) Examples of bursts collected in 300-μs bins, showing counts in donor and acceptor channels.

flexible, permitting the N-terminal and C-terminal domains to adopt a wide distribution of relative conformations to accommodate different targets (*14*, *15*), allowing for the promiscuous binding interactions of CaM.

The structure adopted by CaM in solution, and the possible heterogeneity of CaM conformations, have been the subject of extensive debate. Early crystal structures of Ca^{2+}-CaM predicted an extended, helical linker separating the opposing domains (*8*, *16*). However, multiple studies of CaM revealed a different picture, including NMR studies that observed significant flexibility of the central linker (*14*, *17*−*19*), and computational (*20*, *21*) and fluorescence studies (*22*, *23*) that predicted a more compact structure due to a bend in the central linker. Recently, a much different crystal structure of Ca^{2+}-CaM has been published, this one very compact with opposing domains in close proximity (*11*). A solution structure of CaM in the absence of Ca^{2+} (apoCaM) has also been published (*12*) and predicts less ordered domains separated by ~30−40 Å, which agrees well with computational (*24*) and fluorescence studies (*22*, *23*). NMR, X-ray crystallography, and fluorescence studies suggest a high degree of disorder, leading to speculation that multiple conformations of Ca^{2+}-CaM and apoCaM are present in solution (*10*, *12*, *18*, *22*, *25*, *26*).

Single-molecule spectroscopy provides a method for uncovering conformational substates and heterogeneity that may be hidden by the ensemble averaging of conventional methods (*27*−*29*). Single-molecule FRET is particularly useful because it reports the distance between two probes and can be used to monitor target binding, motions between opposing protein domains or DNA subunits, and heterogeneity of structure (*30*−*33*). Moerner and co-workers demonstrated the ability to observe Ca^{2+}-dependent conformational changes and dynamics of target binding of CaM by spFRET with a CaM-chameleon, a construct consisting of cyan and yellow mutants of green fluorescent protein separated by CaM and the CaM-binding domain of myosin light chain kinase (*34*). Recently, single-molecule studies in the laboratory of Lu and co-workers examined nanosecond domain motions in CaM (*35*), and Hochstrasser and co-workers studied interactions between CaM and an amphiphilic peptide (*36*). In our laboratory, we generated a doubly labeled CaM mutant with cysteines substituted at residues 34 and 110 conjugated with the single-molecule FRET pair AlexaFluor 488 and Texas Red (*37*, *38*). We used this construct to obtain single-molecule distributions of freely diffusing, doubly labeled CaM molecules in solution by measuring relative donor and acceptor fluorescence intensity (*9*). These relative intensities were used to obtain the FRET efficiency and corresponding distance between residues 34 and 110 and, thus, between the N- and C-terminal domains of single CaM-DA molecules. Multiple conformations were observed for both Ca^{2+}-CaM-DA and apoCaM-DA, including one with a distance between residues 34 and 110 of around 38 Å and another centered around 55 Å. A third conformational substate was observed at a shorter distance, around 29 Å.

In-depth understanding of the dependence of conformational substates upon biologically relevant solution conditions is needed for increased understanding of the participation of CaM in diverse signaling pathways. The results presented in the current study show population shifts in the conformational substates of CaM as a function of Ca^{2+}, notably, a decreased amplitude of an extended structure with increasing Ca^{2+}. In addition, changes in the conformational substates of CaM-DA were observed at low pH, in helix-inducing solvent, and at low ionic strength. The changes in conformation of CaM-DA at low pH are particularly interesting, given that a number of CaM-dependent enzymes show changes in activity at varying pH values, including myosin light chain kinase (MLCK) (*39*), phosphorylase kinase (*40*), and calcineurin (*41*). We propose that multiple conformations of CaM may play a role in CaM's ability to interact with diverse targets, and hypothesize that electrostatic interactions between acidic residues in CaM contribute to determine the nature of the lowest energy conformation in solution. Electrostatic interactions between these residues are dependent on pH, therefore we hypothesize that the influence of pH on CaM conformation may play a role in the pH-dependent CaM recognition of some enzymes.

CaM isolated from aged rat and CaM oxidized by H_2O_2 has been shown to possess a decreased ability to activate the plasma membrane Ca^{2+} ATPase (*42*, *43*), and the reversible oxidation of methionines was suggested to have implications in Ca^{2+} homeostasis for cells undergoing

oxidative stress (*44*−*46*). Therefore, it is important to fully understand the structural changes of CaM upon methionine oxidation. We found that continued oxidation of methionine residues in CaM-DA led to an increase in an extended population of CaM-DA, with opposing globular domains separated by over 50 Å.

MATERIALS AND METHODS

Sample Preparation. CaM T34/110C was expressed, purified, fluorescently labeled, and separated following methods described previously (*37*, *38*, *47*). Briefly, threonine residues 34 and 110 of chicken CaM (CaM T34/110C) were mutated to cysteines by a PCR method previously described (*48*, *49*). The expression vector for CaM T34/110C was inoculated in *Escherichia coli* and grown in a standard M9 medium. The culture was harvested and the CaM mutant was purified using a Phenyl Sepharose CL-4B resin. The purified CaM T34/110C was labeled simultaneously with Alexa Fluor 488 maleimide (AF488) and Texas Red maleimide (TR) (Molecular Probes, Eugene, OR), and the double-labeled construct CaM-DA was separated by reverse phase HPLC with a C5 Bio Wide Pore column and a standard acetonitrile, water gradient. For anisotropy studies, the CaM-T34C and CaM-T110C constructs were labeled with AF488 or TR, and free dye was removed by gel filtration or extensive dialysis. Purity of singly and doubly labeled CaM constructs was verified via mass spectrometry. Control experiments in our laboratory have shown little or no effect of dye conjugation to CaM in regard to interaction with or activation of target enzymes (refs *38* and *50* and unpublished results).

Experimental Setup. Buffer conditions for the Ca^{2+}-dependent experiments consisted of 10 mM HEPES, pH 7.4, 0.1 M KCl, 1 mM $MgCl_2$, 0.1 mM $CaCl_2$ (buffer K). To set Ca^{2+} concentrations, buffers of varying concentrations of EGTA were made with dilutions from a stock buffer consisting of buffer K plus 3.0 mM EGTA. From this stock, dilutions with buffer were made for a range of final EGTA concentrations of approximately 300, 150, 130, 120, 110, 105, 100, 95, and 0 μM EGTA. The free Ca^{2+} concentrations of the buffer solutions were verified by titration using the Ca^{2+} indicators calcium green-1 and 5,5′-dibromo-BABTA and standard Ca^{2+} buffers at identical Mg^{2+}, pH, and ionic strength (Molecular Probes, Eugene, OR). The corresponding experimental free Ca^{2+} concentrations were found to be 0.150, 0.590, 1.0, 2.1, 5.5, 8.2, 12.9, 17.6, and 100 μM, respectively. For studies at low ionic strength, CaM-DA was dialyzed against 10 mM HEPES, pH 7.4, and 0.1 mM $CaCl_2$, in the presence of and absence of 300 μM EGTA. For studies of oxidative modification, CaM mutants were oxidized after fluorescence labeling according to published protocols (*42*, *51*). Briefly, CaM-DA was incubated in approximately 100 mM H_2O_2 under saturating Ca^{2+} for a period of 14 h or 24 h. After incubation, excess H_2O_2 was removed by extensive dialysis, and oxidized samples were diluted with appropriate buffers to vary the free Ca^{2+} concentration. For studies at reduced pH, the pH of buffer K was adjusted with 1 M HCl and measurements were taken immediately. For studies in 50% ethanol, a stock buffer was diluted with ethanol and the pH adjusted if necessary.

The 488 nm line of an Ar^+/Kr^+ laser (Lexel) was directed into the back of an inverted fluorescence microscope (Nikon TE2000). The beam was reflected with a dichroic mirror (Q505LP, Chroma Technologies) onto a 1.3 NA, 100X oil-immersion objective (SuperFluor). The excitation power at the entrance of the objective was 35 μW. The objective collected the emission, which passed through the same dichroic mirror and out the side port of the microscope. A dichroic filter (565DCLP, Chroma Technologies) was used to separate the donor and acceptor fluorescence emission. Band-pass filters were placed in front of the donor (HQ525/50M, Chroma Technologies) and acceptor (HQ620/75M, Chroma Technologies) detectors. Single-photon counting avalanche photodiodes (SPCM-ARQ-14, Perkin-Elmer) were used to count the fluorescence photons.

Analysis of FRET Distributions. A drop of CaM-DA at a concentration of approximately 100 pM was placed on a microscope slide above the objective. The beam was focused at a minimum of 20 μM above the surface. At this distance above the surface, fluorescence from molecules that may have adhered to the glass surface was rejected. As single molecules traversed the focal region, fluorescence was obtained in donor and acceptor channels separately in 300-μs bins. Relative donor and acceptor counts in a spFRET system can be used to determine the spatial separation between the probes averaged over the time bin of the data collection (*52*, *53*). Using this method with dilute, freely diffusing CaM-DA, the vast majority of the time there was no molecule in the focal region, and very few counts were obtained. A cutoff method was used similar to those described previously to determine the presence of a molecule in the focal volume (*9*, *54*). For inclusion of a bin, it was required that the donor or acceptor counts be larger than 8 times the standard deviation of the background signal in each channel separately, or that the sum of donor and acceptor counts be 6 times above the sum of the donor and acceptor background level. The distributions differ slightly from those previously published (*9*) because the excitation power was lower and the bin size was larger, decreasing the apparent noise and allowing for cleaner comparison and observation of multiple conformations. In addition, donor bleed-through into the acceptor channel (roughly 10%) was subtracted from the acceptor. It was required that acceptor counts be above background after subtraction of donor bleed-through (roughly 10%) in an attempt to avoid inclusion of bins that may be biased toward low FRET efficiency due to acceptor photobleaching. This cutoff method requires a high signal-to-background ratio, decreasing the contribution of Poisson counting noise to the uncertainty in calculated FRET efficiency.

The determination of cutoffs is necessarily somewhat arbitrary in nature, but allows for direct comparison between distributions collected with identical cutoff parameters. That is, differences in distributions obtained with identical experimental setups that implement identical cutoff parameters can be quantitatively analyzed. Use of these cutoffs also resulted in distributions whose average matched the average FRET efficiencies obtained form bulk data. Slight adjustment of cutoff parameters did not significantly alter the distributions. The day-to-day drift in the relative detection efficiency of the two channels was minimal and led to shifts in the peaks of the distributions on the order of 1−2 Å, adding to the widths of the measured distributions. Increased bin size up to 1 ms did not significantly alter the distributions.

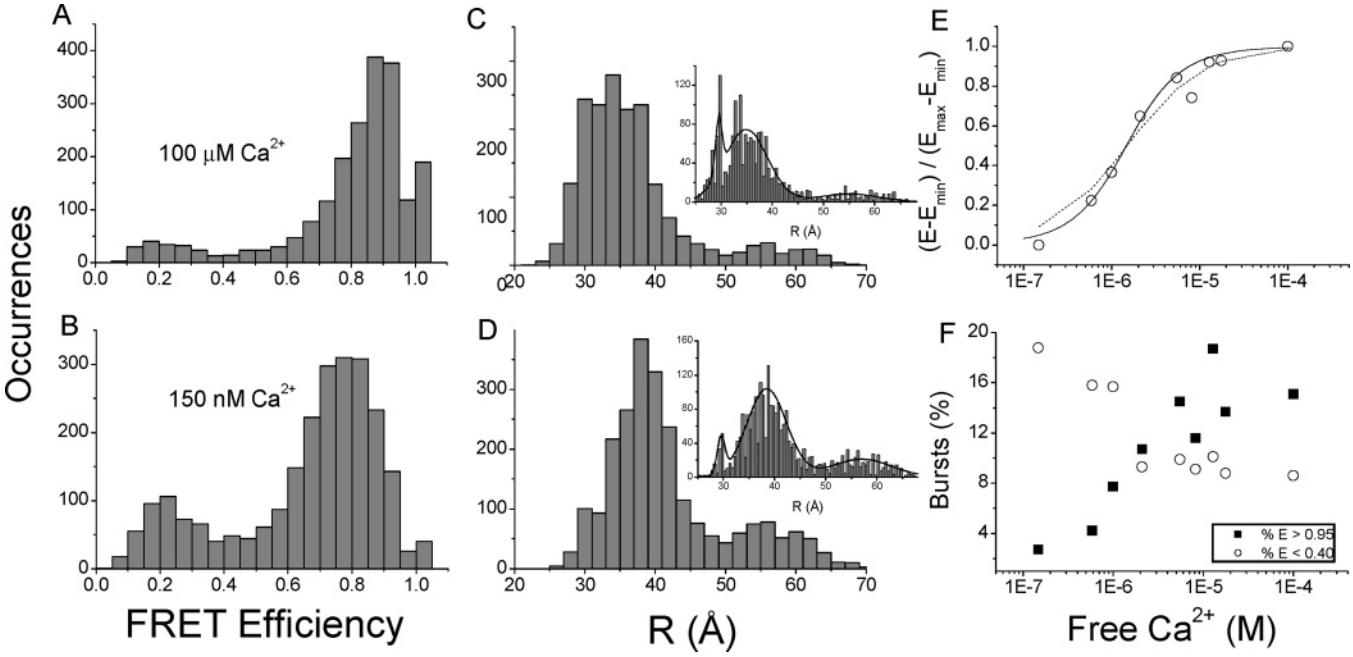

FIGURE 2: (A, B) FRET efficiency distribution of bursts that meet the signal-to-noise selection criteria taken at 100 μM Ca^{2+} (A) and 150 nM Ca^{2+} (B). (C, D) Corresponding distance distributions with bin sizes of 2 Å and 0.5 Å (inset) at 100 μM Ca^{2+} (C), and 150 nM Ca^{2+} (D). Gaussian fits to the distributions are shown to demonstrate the multiple substates of CaM. (E) Average FRET efficiency (normalized, see eq 4) of bursts as a function of free Ca^{2+} with the fit to a two-site, cooperative model (eq 3) (solid line). A fit to a noncooperative, two-site model with equal Ca^{2+} binding affinities is shown with a dotted line. (F) Percentage of bursts below FRET efficiency 0.40 (○) and above 0.95 (■) as a function of free Ca^{2+}.

Once it was determined that donor and/or acceptor counts were high enough to ensure that a molecule was present in the focal region, the FRET efficiency for a single bin was found from the equation

$$E = \frac{c(I_a - bI_d)}{c(I_a - bI_d) + I_d} \quad (1)$$

where c is a factor to correct for relative detection efficiency of the donor and acceptor and b is a correction for average bleed-through from the donor to acceptor channel. The determination of c has been discussed in detail elsewhere (*37*).

From the FRET efficiency, distances (R) were obtained according to

$$R = \left(\frac{1 - E}{E}\right)^{1/6} R_0 \quad (2)$$

where R_0 is the Förster distance, or distance of 50% energy transfer between donor and acceptor. For AF488 and TR, an R_0 of 46.5 Å was calculated from the spectral overlap of the donor fluorescence and acceptor absorption (*55*). In conversion of the FRET efficiency distributions to distance distributions, some bins were obtained with $E = 1.0$ due to zero donor counts. According to eq 2, these occurrences of high FRET correspond to an unrealistic distance of 0 Å, and thus were not included in the distance distributions.

Time-Resolved Fluorescence. Time-resolved fluorescence spectroscopy was carried out by time-correlated single photon counting (TCSPC) with an instrument that has been described previously (*56*). A mode-locked, frequency-doubled Nd:YAG laser (Coherent Antares) synchronously pumped a home-built Rhodamine 6G dye laser operated at 590 nm and cavity-dumped at 3.8 MHz for excitation of Texas Red. A 440-nm picosecond pulsed diode laser (LDH 440, Picoquant GmbH) was operated at 10 MHz for excitation of AF488. A monochromator band-pass of 10 nm was used for all time-resolved experiments. Emission was collected at 612 nm for TR. The emission of AF488 was collected slightly off peak, at 525 nm, to reduce the contribution from Raman scattering. All intensity decays were collected with a polarization at 54.7° from vertical. A correction factor for normalization of the collection intensity of parallel and perpendicular anisotropy decays was obtained by comparison of integrated decay intensities with the steady-state anisotropy values. Globals Unlimited decay analysis software (Laboratory for Fluorescence Dynamics, University of Illinois at Urbana−Champaign) was used for data analysis. The fit to the decays was convoluted with an instrument response function collected using scatter from a solution of nondairy creamer. The support-plane method was used to obtain estimates of error limits at one standard deviation (*57*, *58*).

RESULTS

Conformational Substates of CaM. A typical data set is shown in Figure 1B. Bins with high counts in donor and/or acceptor channels correspond to occurrences when a single CaM-DA molecule traversed the focal region. After data collection, the cutoff methods discussed above were implemented to obtain single-molecule FRET efficiency distributions. Each occurrence in the distribution coincides with the FRET efficiency of a 300-μs bin that surpassed the cutoff criteria. Multiple conformational substates are evident in the FRET efficiency distributions (Figure 2A,B) as peaks centered around $E = 0.85$ in Ca^{2+}-saturated CaM-DA, and $E = 0.80$ in apo-CaM-DA, along with a much smaller distribution centered around $E = 0.20$. The FRET efficiency peaks correspond to peaks in the distance distributions

(Figure 2C,D) around 34 Å (Ca^{2+}-CaM-DA) or 38 Å (apoCaM-DA) and 55 Å. The use of a smaller binning size (insets to Figure 2C,D) revealed the presence of an additional component in the data centered at ~28 Å, with a much higher amplitude in the presence of Ca^{2+}. The larger bin size in Figure 2C,D averaged over this additional component, but still allowed for clear identification of two main conformations. As the goal of the current paper was to examine large scale conformational changes at varying conditions, rather than to resolve the difference between the two distributions at 29 and 34−38 Å, a bin size of 2 Å was used for the distance distributions to reduce uncertainty and facilitate comparison of distributions.

Ca^{2+} Dependence of Conformational Distributions. Figure 2E plots the average FRET efficiency of all bursts meeting the selection criteria as a function of free Ca^{2+}. The majority of the change in FRET efficiency occurred over the range of 500 nM to ~3 μM free Ca^{2+}. This is a range consistent with Ca^{2+} binding to the C-terminal domain (*7*, *59*), and there was little change in FRET efficiency over the range of free Ca^{2+} necessary for binding to the lower affinity, N-terminal domain (~10 μM) (*7*, *60*, *61*). Thus, the change in distance between residues 34 and 110 was responsive to Ca^{2+} binding to the C-terminal domain of CaM-DA but not the N-terminal domain. The observed changes in FRET efficiency over this Ca^{2+} range were therefore analyzed in terms of Ca^{2+} binding to two cooperative sites in the C-terminal domain. Following Shea and co-workers (*7*, *59*, *62*), we fit the FRET efficiency curve to a two site binding function,

$$E_n = \frac{K_1[Ca^{2+}] + 2K_2[Ca^{2+}]^2}{2(1 + K_1[Ca^{2+}] + K_2[Ca^{2+}]^2)} \quad (3)$$

where $[Ca^{2+}]$ is the free Ca^{2+} concentration, K_1 is the sum of the equilibrium constants k_1 and k_2 for Ca^{2+} binding to the two binding sites in the C-terminal domain, and K_2 is the equilibrium constant for Ca^{2+} binding to both sites. E_n represents the FRET efficiency normalized from 0 to 1 to form the curve in Figure 2E:

$$E_n = \frac{E - E_{min}}{E_{max} - E_{min}} \quad (4)$$

E_{max} is the FRET efficiency at 100 μM Ca^{2+} (0.793), and E_{min} is the FRET efficiency at 150 nM Ca^{2+} (0.654). The fit to eq 3 (Figure 2E) yielded $K_1 = 5.98 \times 10^5\ M^{-1}$ and $K_2 = 4.64 \times 10^{11}\ M^{-2}$, corresponding to free energies of Ca^{2+} binding ($\Delta G_2 = -15.6 \pm 0.1$ kcal mol^{-1}, $\Delta G_1 = -7.7 \pm 0.1$ kcal mol^{-1}) that are consistent with values reported by Shea and co-workers for the free energy of Ca^{2+} binding to the C-terminal domain of CaM, yet are distinct from values reported for Ca^{2+} binding to the N-terminal domain (*7*, *59*, *61*). A fit to a Hill plot (not shown) yielded a Hill coefficient of 1.3, suggesting some cooperativity in Ca^{2+} binding to the C-terminal domain sites. Also shown in Figure 2E is the fit assuming $k_1 = k_2$ and no cooperativity between Ca^{2+} binding sites ($K_2 = k_1^2$) (dotted line).

An interesting feature of the distributions is the Ca^{2+} dependence of the amplitude of the state with lower FRET efficiency. The decreased excitation intensity and larger integration time used in the current study led to a decreased likelihood of acceptor photobleaching during the transit time, lowering the amplitude of occurrences of low FRET efficiency relative to our earlier study (*9*) and revealing a decreased amplitude of the extended conformation at increasing Ca^{2+} concentration. This is illustrated in Figure 2F as the fraction of molecules having FRET efficiency below 0.40 as a function of free Ca^{2+}. This fraction gradually decreased as the Ca^{2+} concentration was increased from 150 nM Ca^{2+} to 1.0 μM Ca^{2+}, followed by an abrupt drop at 2.1 μM Ca^{2+}. Another difference in the distributions is represented by a shift in the percentage of bursts above $E = 0.95$, shown in the black in Figure 2F. This effect is more gradual over the free Ca^{2+} range. Although examination of bulk emission spectra could reproduce the results of Figure 2E (average FRET efficiency as a function of free Ca^{2+}), the results presented here show that the change in average distance is due to a shift in a high FRET efficiency conformational substate toward a higher FRET efficiency upon an increase in Ca^{2+} concentration, along with a decrease in amplitude of a distribution centered at $E = 0.20$.

Effect of Solution Conditions on CaM Conformations. Figure 3A−D shows the distance distributions of individual bursts for CaM-DA at low pH, Ca^{2+}-CaM-DA in 50% ethanol, and apoCaM-DA at low ionic strength. Figure 3A,B demonstrates the change in conformation of CaM-DA at pH 5.0. The distributions in Figure 3A (pH 5.0, 100 μM Ca^{2+}) and 3B (pH 5.0, 150 nM Ca^{2+}) were shifted to shorter distance (high FRET efficiency), with fewer than 10% of the bursts yielding a distance longer than 38 Å. There was no observed Ca^{2+} effect on the distributions at low pH. This is in contrast to all other conditions tested, which showed an increase in average FRET efficiency in the presence of Ca^{2+}. The change in FRET efficiency at low pH can be interpreted in terms of the change in stability of the central helix upon disruption of interactions that favor helix formation (see Discussion).

Alcohols are known to induce helix formation in CaM (*63*, *64*). To examine the effect of alcohol on the distance between residues 34 and 110, the distribution of CaM-DA at saturating Ca^{2+} levels in the presence of 50% ethanol was obtained (Figure 3C). The distribution is very broad but shows no clear indication of multiple conformations. The average FRET efficiency was lower ($E = 0.56$) relative to CaM-DA in the absence of ethanol. The distribution of CaM-DA at 150 nM Ca^{2+} and low ionic strength (in the absence of KCl and $MgCl_2$, ionic strength ~ 0.0001) is shown in Figure 3D. While two distributions are still evident, the distribution changed significantly from that found at low Ca^{2+}, high ionic strength (150 nM Ca^{2+}, 100 mM KCl, 1 mM $MgCl_2$) in Figure 2D. There appears to still be a conformation centered at ~38 Å, but with the decrease in ionic strength it decreased in amplitude relative to the long distance distribution. The two distributions are less well resolved in Figure 3D, suggesting a change in the structure of CaM at low ionic strength that may be related to interactions between residues in the central linker (see Discussion). In addition, while the average distance was longer at low ionic strength, the percentage of bursts at distance <32 Å was increased at low ionic strength (Figure 3D) relative to apoCaM-DA at high ionic strength (Figure 2D) (27% vs 11%), representative of an increase in conformational heterogeneity at low ionic strength. A distribution with the same low ionic strength

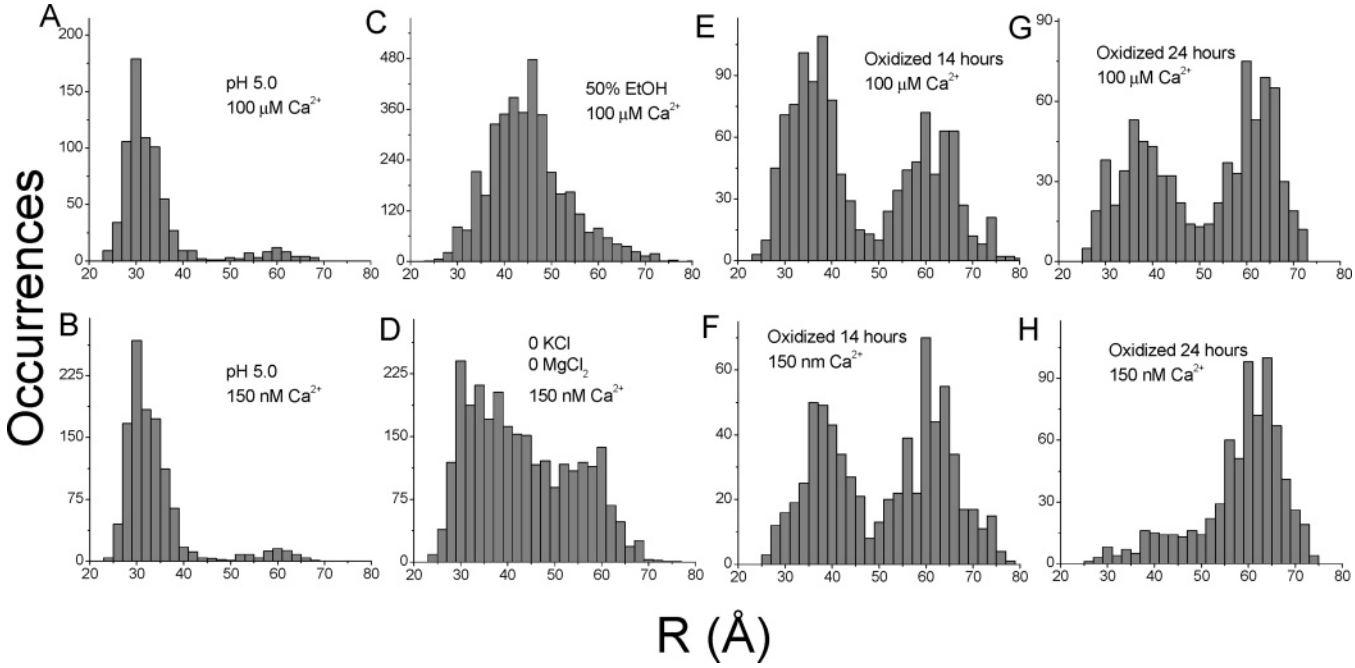

FIGURE 3: (A, B) Distance distributions of CaM-DA at pH 5.0 at 100 μM Ca^{2+} (A) and 150 nM Ca^{2+} (B). (C) Distance distribution of CaM-DA in the presence of 50% ethanol. (D) Distance distribution of CaM-DA at low ionic strength (in the absence of KCl and $MgCl_2$), at 150 nM free Ca^{2+}. (E−H) Distance distributions of CaM-DA after oxidation for 14 h (E, F) and after 24 h (G, H) in the presence of 100 μM free Ca^{2+} (E, G) and 150 nM free Ca^{2+} (F, H).

conditions except at 0.1 mM free Ca^{2+} (ionic strength ~ 0.0003) was also obtained (not shown) but showed no significant change from the high Ca^{2+} distribution at high ionic strength (0.1 M KCl, 1.0 mM $MgCl_2$).

Conformations of Oxidized-CaM. Figure 3E−H shows the distance distributions of individual bursts for oxidized CaM-DA. Oxidation of CaM-DA was carried out at a saturating Ca^{2+} concentration, and the sample was then dialyzed and diluted with appropriate buffers to obtain the desired Ca^{2+} level. The sample was not oxidized separately under low and high Ca^{2+} conditions, and thus the results in Figure 3 do not address the possible difference in exposure of methionines to oxidation at high and low Ca^{2+} concentrations. Figure 3E,F shows the distributions at 100 μM Ca^{2+} and 150 nM Ca^{2+} for CaM-DA that had been oxidized for 14 h under the conditions outlined above, while Figures 3G,H shows the distributions obtained after oxidation of CaM-DA for 24 h. The distributions of oxidized CaM-DA display a similar Ca^{2+} dependence as unoxidized CaM-DA in that the average FRET efficiency was higher in the presence of saturating Ca^{2+} than in the absence (confirmed by ensemble measurements; not shown). There are still two main conformations, one centered around $R = 38$ Å, and one centered around $R = 60$ Å. The long distance (low FRET efficiency) peak was shifted a few angstroms toward longer separation in oxidized CaM-DA relative to unoxidized CaM-DA. The most pronounced change upon oxidation was in the amplitudes of the two main conformations. A trend toward increased probability of an extended conformation upon prolonged oxidation is apparent. In CaM-DA that has been oxidized for 14 h (Figure 3E,F) the peak at long distance has an amplitude of around 50%. Upon oxidation for 24 h (Figure 3G,H) the extended conformation dominates the distributions, and the peak around 38 Å is much lower in amplitude, and nearly absent in apoCaM-DA. This could be a result of oxidation of a larger fraction of methionine residues with longer peroxide exposure. Alternatively, oxidation of one or two residues may be responsible for formation of the extended conformation, with a larger percentage of these being oxidized as the exposure time is extended (see Discussion).

Dye Reorientational Dynamics. In SpFRET studies, it is important to take into consideration dye behavior and its possible influence on results (*65*). In particular, the possibility of coupling of dye motion to protein domains was examined to ensure that the relative orientations of the donor and acceptor dipoles were adequately averaged over the time scale of the measurement (*66*, *67*). The extent of reorientational freedom of dyes can be assessed by measurement of the steady-state anisotropy (r_{ss}):

$$r_{ss} = \frac{I_{||} - I_{\perp}}{I_{||} + 2I_{\perp}} \tag{5}$$

where $I_{||}$ and $I_{\perp}$ are vertically and horizontally polarized emission intensities following vertically polarized excitation. Likewise, time-resolved collection of vertically and horizontally polarized emission can be used to obtain the time-resolved anisotropy ($r(t)$),

$$I_{||}(t) = \frac{1}{3}I(t)[1 + 2r(t)] \qquad I_{\perp}(t) = \frac{1}{3}I(t)[1 - r(t)] \tag{6}$$

The time-resolved anisotropy is often described by the sum of multiple processes,

$$r(t) = \sum_j r_{0_j} \exp(-t/\theta_j) \tag{7}$$

where r_{0_j} is the anisotropy in the absence of rotational diffusion and θ_j is the rotational correlation time for the jth component. A lower steady-state anisotropy, or a faster

Table 1. Lifetimes and Steady-State and Time-Resolved Anisotropies for Singly Labeled CaM Species

sample	τ_f (ns)	r_{ss}	a_1	τ_{r1} (ns)	a_2	τ_{r2} (ns)
			CaM-T34C-AF488			
high calcium	4.19 ± 0.02	0.12	0.49 ± 0.06	0.7 ± 0.2	0.51 ± 0.06	7^{+1}_{-1}
apo	4.20 ± 0.02	0.12	0.50 ± 0.07	0.8 ± 0.2	0.50 ± 0.07	8^{+2}_{-1}
apo-low ionic strength	4.18 ± 0.02	0.11	0.56 ± 0.06	0.7 ± 0.1	0.44 ± 0.06	7^{+2}_{-1}
oxidized	4.23 ± 0.02	0.11	0.64 ± 0.07	0.9 ± 0.2	0.36 ± 0.07	10^{+5}_{-3}
low pH	4.17 ± 0.02	0.14	0.51 ± 0.05	0.7 ± 0.1	0.49 ± 0.05	8^{+2}_{-1}
50% ethanol	3.99 ± 0.02	0.16	0.60 ± 0.05	1.0 ± 0.1	0.40 ± 0.05	16^{+7}_{-4}
			CaM-T34C-Texas Red			
high calcium	4.74 ± 0.03	0.23	0.4 ± 0.2	2 ± 1	0.6 ± 0.2	14^{+10}_{-3}
apo	4.67 ± 0.03	0.20	0.4 ± 0.1	1.5 ± 0.6	0.6 ± 0.1	12^{+5}_{-2}
apo-low ionic strength	4.78 ± 0.02	0.20	0.4 ± 0.1	1.7 ± 0.5	0.6 ± 0.1	12^{+4}_{-2}
oxidized	4.70 ± 0.03	0.18	0.31 ± 0.06	0.7 ± 0.3	0.69 ± 0.06	8^{+1}_{-1}
low pH	4.74 ± 0.03	0.20	0.24 ± 0.09	1.0 ± 0.5	0.76 ± 0.09	9^{+2}_{-1}
50% ethanol	4.44 ± 0.02	0.14	0.61 ± 0.04	0.9 ± 0.1	0.39 ± 0.04	14^{+4}_{-3}

anisotropy decay, represents increased reorientation of the fluorophore on the time scale of the fluorescence lifetime.

We measured steady-state and time-resolved anisotropies for the singly labeled CaM-T34C mutants (Table 1). In most cases, anisotropy decays were measured for the donor or acceptor fluorophore attached to the 34-site mutant only. We found for a range of solution conditions that the anisotropies did not differ significantly for labeling at the 34 or 110 site, i.e., fluorescence lifetimes, steady-state anisotropies, and time-resolved anisotropies were very similar between CaM-T34C-AF488 and CaM-T110C-AF488, or between CaM-T34C-TR and CaM-T110C-TR (ref *9* and unpublished data). The time-resolved anisotropy of CaM-T34C-AF488 differs slightly from our previous result (*9*) due to an improved deconvolution of the instrument response function for the 440-nm diode laser.

The likelihood of AF488 and Texas Red orientation affecting the observation of multiple conformations is small and has been discussed at length (*9*). Relative orientation of donor and acceptor dipoles contributed little uncertainty to the FRET efficiency of CaM-DA due to rapid reorientation of the donor dipole. Furthermore, fluorescence decays of singly labeled, single-mutant CaM-T34C and CaM-T110C samples were single-exponential, suggesting a homogeneous dye environment. The anisotropies of CaM-AF488 were the same within uncertainty regardless of Ca^{2+} concentration, as were the anisotropies of CaM-TR. The significant amplitude of fast rotational motion of AF488 ensured random orientation of the donor dye relative to the acceptor dye, and maximum uncertainties in the distance measurements due to the averaging of κ^2 were small, on the order of 10−15% (*67*), corresponding to uncertainties in R values on the order of 3 to 8 Å. The motion of AF488 on its C5 linker arm was likely on a time scale much faster than our integration time and therefore did not affect the observance of multiple conformations, though the measured distance may have been offset from the actual distance between residues 34 and 110 by 5−10 Å due to the length of the AF488 linker arm. Texas Red was strongly coupled to the protein and had only a C2 linker; therefore its motion or location affected the distributions only minimally.

Reference to Table 1 shows that it is unlikely that any changes in protein−dye interactions upon oxidation contributed to the observed distribution changes. Steady-state anisotropies of CaM-T34C-AF488 and CaM-T34C-TR did not appreciably change upon oxidation. Amplitudes of the fast and slow rotational correlation times of oxidized CaM-T34C-TR were within error margins of the values for unoxidized CaM-TR, although the rotational correlation times themselves were faster. The faster value of τ_{r2} for oxidized CaM-T34C-TR and CaM-T34C-AF488 probably represents a global change in motion of the protein upon oxidation. The faster time of the fast rotational correlation time τ_{r1} of CaM-T34C-TR upon oxidation (0.7 ns compared to 2 ns for unoxidized CaM) was likely representative of decreased coupling between Texas Red and the protein. More important for comparison are the fluorescence lifetimes, as oxidation was carried out after fluorescent labeling and could possibly have affected the fluorescence properties of AF488 and Texas Red. However, fluorescence lifetimes of both donor and acceptor were unchanged after prolonged exposure to H_2O_2. Combined with the fact that count levels for single-molecule bursts also were unchanged, it is unlikely that the oxidation process altered dye photophysics.

Fluorescence lifetimes of donor and acceptor remain the same within uncertainty at reduced pH. Steady-state anisotropies also did not differ by a substantial amount. The rotational correlation times of Texas Red at site 34 were slightly faster at low pH relative to pH 7.4, with a slightly increased amplitude of global motion. Very little change was observed in the anisotropies of CaM-T34C-TR and CaM-T34C-AF488 in apoCaM at low ionic strength relative to high ionic strength. The time-resolved anisotropy of CaM-T34C-TR in 50% ethanol displayed a larger amplitude of segmental dye motion relative to native conditions, representative of decreased coupling between the dye and CaM. Importantly, there was no evidence from the lifetime and anisotropy data to suggest that protein−dye interactions influenced the distributions. The segmental motion of AF488 was sufficient to ensure low uncertainty in κ^2, and the single-fluorescence lifetimes of CaM-T34C-AF488 and CaM-T34C-TR at all solution conditions suggest homogeneous protein−dye interactions.

DISCUSSION

Conformational Substates of CaM. Heterogeneity of structure of CaM has been inferred by multiple methods, including X-ray crystallography and NMR (*10*, *18*). Crystal

structures of Ca^{2+}-CaM were reported showing an extended, helical central linker (*8*, *10*, *16*) with a distance between residues 34 and 110 of over 50 Å. In contrast, a recently reported structure reveals a compact structure, with the two domains of CaM in close proximity as a result of a bend in the central linker (*11*). Another indication of conformational substates of CaM surfaced in ensemble FRET measurements. Török and co-workers found that two lifetimes were required to fit the fluorescence decay of the donor IAEDANS in the presence of Ca^{2+} and the acceptor *N*-[4-(dimethylamino)-3,5-dinitrophenyl] maleimide (DDP) (*22*), with an amplitude of 75% corresponding to a distance of 40 Å between probes at sites 34 and 110 and an amplitude of 25% corresponding to a distance of 25 Å.

Conformational distributions determined by spFRET provide clear evidence of conformational substates (*9*). Resolution of conformational substates by spFRET permits examination of the response of the populations of individual conformational states to solution conditions. Multiple, distinct, subconformations are populated in both Ca^{2+}-CaM-DA and apoCaM-DA at room temperature and persist for at least hundreds of microseconds. Figure 2C,D illustrates the distinct subconformations of CaM-DA at 100 μM Ca^{2+} and 150 nM Ca^{2+}. At least three stable conformations of Ca^{2+}-CaM-DA can clearly be observed in solution (insets to Figure 2C,D). The most compact conformation corroborates the short lifetime component reported by Török and co-workers (*22*). Distributions obtained with a larger bin size of 2 Å demonstrate clearly the changes in the two main conformations upon changes in solution conditions, but the most compact conformation was not resolved with bins this large.

Effect of Ca^{2+}. Figure 2E reports the average FRET efficiency as a function of free Ca^{2+} for all bins above the cutoff criteria. The average FRET efficiency increases with the increase in Ca^{2+}, partially due to decreased occurrences of low FRET efficiency (long distance) states (Figure 2E,F). The results in Figure 2E can be understood in light of previous work on Ca^{2+} binding to CaM. Forsén and co-workers observed a 6-fold higher Ca^{2+}-binding affinity for the C-terminal fragment of CaM relative to the N-terminal fragment (*68*). Shea and co-workers examined intrinsic tyrosine and phenylalanine fluorescence in CaM, taking advantage of their sensitivity to Ca^{2+} binding to determine Ca^{2+} affinity of the N- and C-terminal domains of CaM. They observed Ca^{2+}-dependent fluorescence changes of Tyr138 in the C-terminal domain of vertebrate-CaM and *Paramecium*-CaM at Ca^{2+} concentrations on the μM range (*7*, *60*, *69*). In studies of the N-domain of CaM (*60*, *61*), phenylalanine fluorescence was most responsive over a Ca^{2+} range nearly an order of magnitude higher, around 10 μM.

The majority of the change detected in the FRET efficiency occurred over the range of 500 nM to ~3 μM free Ca^{2+} (Figure 2E), a range consistent with Ca^{2+} binding to the C-terminal domain (*7*, *59*). Ca^{2+}-dependent shifts in the relative populations of the compact and extended conformations of CaM-DA (Figure 2C,D) indicate global structural changes in CaM, suggesting that it is not just the C-terminal domain of CaM that is involved in Ca^{2+}-dependent conformational changes over this range. Therefore, Ca^{2+} binding to the C-terminal domain does not simply induce structural changes in that domain, but also induces structural changes that affect the distance between domains, consistent with studies of Shea and co-workers that revealed a change in conformation in the N-terminal domain upon Ca^{2+} binding to the C-terminal domain (*59*), and a change in interactions between domains at intermediate Ca^{2+} levels (*70*). The results reported here are consistent with these studies in that Ca^{2+} binding to the C-terminal domain of CaM induces a global structural change, possibly including reorientation in the central linker, that increases the average FRET efficiency between residues 34 and 110.

The spFRET distributions provide additional information about the nature of the conformational changes upon addition of Ca^{2+} (Figure 2C,D). The distributions show that the change in the average distance upon addition of Ca^{2+} is due in large part to a change in amplitude of an extended conformation that does not shift in distance. Shea and co-workers observed an increase in the Stokes radius of CaM and CaM mutants upon removal of Ca^{2+} (*71*, *72*). The results reported here are in agreement and suggest that the reduced likelihood of the extended conformation and the slight shift in the more compact distribution both contribute to the observed changes in the ensemble measurements.

Structural Changes in 50% Ethanol. The distribution obtained in 50% ethanol at 0.1 mM Ca^{2+} is shown in Figure 3C and can be compared to the distribution at 0.1 mM Ca^{2+} in the absence of ethanol in Figure 2C. The distribution in 50% ethanol is broad, but provides no evidence for the presence of multiple substates. Ethanol is known to decrease hydrogen bonding to solvent, increasing the stability of intramolecular hydrogen bonds and thus favoring helical structures relative to nonhelical. A CD study by Bayley and co-workers showed that alcohol led to an increase in helical content in CaM (*73*). Similarly, Vogel and co-workers examined the backbone dynamics of Ca^{2+}-CaM in 35% trifluoroethanol (*63*) and observed increased rigidity in the central helix, leading them to suggest that the alcoholic conditions used for crystallization unnaturally stabilized the central linker. It is interesting to note that the distribution of Ca^{2+}-CaM-DA in ethanol is centered at 44 Å, which does not correspond to any of the subconformations of Ca^{2+}-CaM-DA in the absence of alcohol (Figure 2C). Thus, it appears that the substates of Ca^{2+}-CaM-DA under native conditions are distinct from the conformation induced in Ca^{2+}-CaM-DA by the presence of ethanol.

CaM-DA at Low pH and Low Ionic Strength. Comparison of Figure 3A with Figure 2C shows a shift in the population to a compact structure at low pH, with few bursts present that correspond to *R* values larger than 40 Å. The distributions also are more narrow at reduced pH, signifying a reduction in conformational heterogeneity, consistent with an ensemble study of Squier and co-workers (*74*). It is interesting to note in Figure 3A,B the absence of a Ca^{2+} effect on the distributions at pH 5. A possible explanation could be a reduced Ca^{2+} affinity for CaM at reduced pH, reported previously (*23*), and that the Ca^{2+} concentration of 0.1 mM used in the current experiments does not saturate the Ca^{2+} sites at low pH. To investigate this possibility, data were taken at 10 mM Ca^{2+}, a 100-fold increase over that used for previous saturating Ca^{2+} distributions (not shown). The distribution was the same within uncertainty as those in Figure 3A,B. Thus, it can be concluded that Ca^{2+} binding has a minimal effect on the distance between residues 34 and 110 at reduced pH. Changes in pH also may change the

interaction between CaM and Mg^{2+} and K^+, and it is possible that these changes contribute to the observed changes in the distribution at reduced pH.

Structural changes at low pH cannot simply be due to a reduction in the C-terminal binding affinity for Ca^{2+}; if this were the case, the low pH distribution should resemble the distribution for apoCaM-DA at pH 7.4 (Figure 2D). Instead, at low pH the distribution shifts toward a more compact structure, in the opposite direction as the shift in distance between residues 34 and 110 in apoCaM-DA relative to Ca^{2+}-CaM-DA. The results are consistent with studies of Shea and co-workers who found a decrease in Stokes radius of CaM at reduced pH (*71*), and suggest that the reduction in amplitude of the extended conformation of CaM at reduced pH contributes to the change in the ensemble average.

The large effect of pH on the distance distributions of CaM-DA is not readily explained by a change in the charge of the only histidine residue (residue 107, $pK_a \sim 6$), as changes in amplitude of conformations separated by nearly 20 Å are likely the result of large scale conformational changes. However, glutamic acid ($pK_a \sim 4$) and aspartic acid ($pK_a \sim 4$) make up a large component of CaM (21 and 17 residues, respectively). There are a particularly large number of glutamic acid and aspartic acid residues in the central linker region, including aspartic acid residues 50, 58, 64, 78, 80, 93, 95 and glutamic acid residues 54, 67, 82, 83, 84, 87. Therefore, a possible explanation for the large pH effect is a change in charge of these residues at pH 5 due to a shift in their pK_a in the presence of clusters of negative charges. Perturbation of the pK_a's of amino acid side chains is a common occurrence in proteins (*75*, *76*), and has been suggested to occur to negatively charged residues in CaM (*23*, *74*).

Previous workers have speculated that electrostatic interactions between glutamic acid and aspartic acid may serve a role in determining the conformation of the central linker region of CaM (*74*, *77*). A number of these residues reside adjacent to the flexible hinge (roughly residues ~73 to 83) (*78*), and electrostatic interactions at neutral pH may increase the relative energy of a structure that places these residues in close proximity. Thus, while these residues are known to interact electrostatically with targets (*4*), the results reported here suggest that these residues may also serve as electrostatic "spacers" in the central linker at physiological pH in the absence of a target. If the charge of one or more side chains in the region is neutralized at pH 5, their ability to act as electrostatic spacers would be curtailed, leading to a more favorable energy of a compact conformation of CaM.

The role of electrostatic interactions can be examined by changing the ionic strength of the solution. We observed an overall increase in average distance for apoCaM-DA at low ionic strength relative to high ionic strength (0.1 M KCl, 1.0 mM $MgCl_2$) (Figure 3D vs 2D). This result is consistent with the idea that electrostatic interactions in the central linker or the globular domains help to define CaM conformation. At low ionic strength and physiological pH, interactions between negatively charged glutamic acid and aspartic acid residues are less shielded than in a buffer at high ionic strength, possibly leading to additional repulsion and an extended interdomain region, and thus a lower average FRET efficiency.

The distribution at low ionic strength still shows evidence of multiple conformations; however, they are less well resolved, and contain additional amplitude on the extreme ends of the distribution relative to the high ionic strength conditions. Thus, while the increase in average distance between domains at low ionic strength is consistent with the hypothesis that electrostatic interactions play an important role in the structure of CaM, the increase in amplitude on each end of the distribution signifies an increase in conformational heterogeneity of apoCaM at low ionic strength, in agreement with an ensemble FRET study between residues 69 and 99 conducted by Squier and co-workers (*74*). A significant change at low ionic strength was not observed for the high Ca^{2+} distribution (not shown) compared to the distribution at high ionic strength and high Ca^{2+} (Figure 2C). The fact that a decrease in ionic strength does not significantly change the single-molecule Ca^{2+}-CaM-DA distribution is more likely an indication that Ca^{2+} binding stabilizes the structure of the linker, rather than a result of the small increase in ionic strength at the elevated free Ca^{2+} levels of Ca^{2+}-CaM relative to apoCaM.

Oxidized CaM-DA. The oxidation of CaM has a dramatic impact on its interaction and activation of targets, and therefore has implications in aging and loss of Ca^{2+} homeostasis (*46*). It has been shown that oxidized CaM is able to bind the plasma membrane Ca^{2+}-ATPase (PMCA) with high affinity (*43*), yet demonstrates a reduced ability to activate the PMCA and functions as an inhibitor of PMCA activity (*42*, *43*, *79*, *80*). Figure 3E−H reveals a dramatic change in the conformations of oxidized CaM-DA relative to unoxidized CaM-DA (Figure 2C and Figure 2B). Comparison of Figure 2C with Figure 3E and Figure 3G and of Figure 2D with Figure 3F and Figure 3H shows an increase in the amplitude of the extended conformation with a longer oxidation period. There also appears to be a shift in the extended conformation to slightly longer distance upon oxidation. It is quite possible that structural changes of CaM upon oxidation are related to changes in activity of CaM toward its targets. One possibility is that the structural changes that lead to the increased population of the extended conformation of CaM could be related to a decreased propensity to form a compact binding complex with a target.

Squier and co-workers showed that the most accessible methionines, and thus the first to be oxidized, are C-terminal methionines 146 and 147 in wheat-germ CaM (*43*), while more recent work demonstrated that oxidation for 24 h results in complete oxidation of all methionines in CaM (*51*). In the current study, oxidation occurred for either 14 h (Figure 3E,F) or 24 h (Figure 3G,H). On the basis of the study by Squier and co-workers (*43*), oxidation of methionines 144 and 145 (analogous to methionines 146 and 147 in wheat-germ CaM) is likely to occur rapidly, and the fact that we see a significant change in structure with longer oxidation times suggests that it is the oxidation of less exposed methionines, possibly methionines 71, 72, or 76 in or near the central linker, that leads to the observed conformational changes.

While oxidized methionine residues in the C-terminus of CaM lead to the decrease in activity of the PMCA, methionine residues in the central portion of CaM are important for determining elasticity and structure (*3*, *10*, *78*). Met 76 is in the middle of a central region of CaM that has

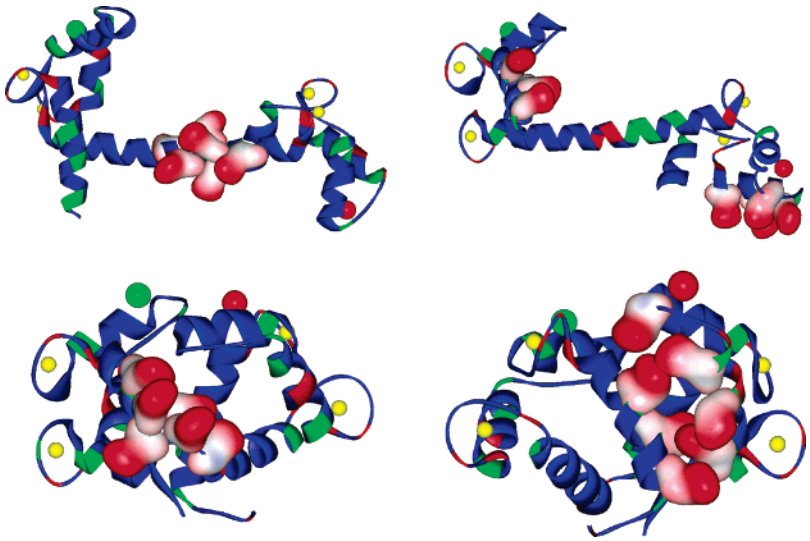

FIGURE 4: Electrostatic surfaces for selected glutamic acid and aspartic acid residues for extended Ca^{2+}-CaM (top row, pdb 1cll (*8*)) and compact Ca^{2+}-CaM (bottom row, pdb 1prw (*11*)) (ViewerPro-4.2, Accelrys, Inc). For the left column, surfaces are shown for residues Asp78, Asp80, Glu82, Glu83, Glu84, and Glu87 in or near the hinge region of the central linker. In the right column, surfaces are shown for Glu residues 7, 11, 14, 114, 120, and 127 near the N-and C-terminal ends of CaM. The remaining glutamic acid (green) and aspartic acid (red) residues are also highlighted.

been shown to be dynamic (*8*, *14*, *78*). The ability of this region to act as a flexible joint and bend upon target binding has been suggested to be important in allowing the opposing domains of CaM to come into close proximity upon target binding (*79*). The significant change in the distributions upon oxidation of methionine residues near the hinge region is consistent with the pH and ionic strength data that suggest the importance of key residues in the linker region in determining overall CaM structure. A study by Means and co-workers examined the effect of methionine to glutamine mutations in CaM binding and activation of smooth muscle MLCK and two forms of CaM-dependent protein kinase (IIa and IV) (*81*). Interestingly, different mutations affected CaM−enzyme interaction differently for the three targets. Mutation of Met 71 and Met 72 lowered the activity of CaM toward MLCK but not toward CaM-dependent protein kinase. Apparently, small changes in structure or hydrophobicity due to changes of individual residues at sites 71 and 72 can have drastically different effects on interactions between CaM and different targets.

The present study shows that oxidation of protected methionine residues in CaM due to prolonged exposure to H_2O_2 affects the positioning of the opposing domains even in the absence of a target, possibly by reducing flexibility in the joint region in a manner that constrains the central linker in a more extended conformation. This finding underscores the importance of key methionine residues in determining CaM structure. However, the present study cannot identify which residues are most responsible for the conformation change. Future studies involving the mutation of selected methionine residues will be required to determine exactly which ones are responsible for the gross change in structure upon oxidation.

Electrostatic Interactions in CaM. The results presented here demonstrate that biologically relevant changes in solution conditions such as pH and ionic strength affect the relative populations of the conformational substates of CaM, raising the question of which residues determine the relative energies of the conformations and thus have a role in determining which is energetically favorable under various biological conditions. Squier and co-workers have suggested that ionizable groups in the central linker are important in determining its structure (*74*). We similarly hypothesize that electrostatic interactions between negatively charged residues have an important role in determining the relative energy and population of multiple conformational substates of CaM. Figure 4 depicts electrostatic surfaces for selected glutamic acid residues and aspartic acid residues in extended Ca^{2+}-CaM from pdb 1cll (*8*) (top row), and in compact Ca^{2+}-CaM from pdb 1prw (*11*) (bottom row). In the left column, electrostatic surfaces for aspartic acid residues 78 and 80 and glutamic acid residues 82−84 and 87 are shown. These residues are either in or adjacent to the flexible hinge region, which must be flexible to allow for motion between domains (*78*). The negatively charged residues in this region are spaced in the extended structure, with all distances between side chain oxygen molecules greater than 7 Å. In contrast, in the compact structure, negatively charged side chain oxygen atoms are much closer, around 4 to 5 Å, due to a bend in this region.

Many charged residues in CaM are involved in forming a negatively charged pocket to stabilize Ca^{2+} binding. Inspection of the crystal structures shows little change in the environment of these residues between the compact and extended CaM structures. However, a number of negatively charged residues are not involved in coordination of Ca^{2+} (glutamic acid residues 7, 11, 14, 114, 120, 123, and 127). These are shown as electrostatic surfaces in the right column of Figure 4. The negative charges are spaced in the extended structure (top row). In order for the compact structure to form, these residues must come into close proximity as a result of a bend in the central linker. The crystal structure of compact Ca^{2+}-CaM (*11*) predicts that the oxygen molecules of the side chains of a number of these glutamate residues are within 4 or 5 Å. Positively charged arginine and lysine residues (not shown) surround the negatively charged surface, but are not placed inside of the region, and thus cannot stabilize the close negative charges.

These observations suggest an importance for electrostatic interactions in determining CaM conformation (*74*), and such interactions may be partially responsible for the presence of multiple substates, a hypothesis that is supported by the marked increase in the relative amplitude of the more compact conformations at low pH. This hypothesis suggests that if multiple conformations of CaM are necessary for its function, electrostatic interactions may govern the relative populations of CaM's conformational substates. This idea could also relate to the pH-dependent activation of a number of CaM-dependent enzymes, including MLCK (*82*), cyclic nucleotide phosphodiesterase (*83*), and the γ-subunit of phosphorylase kinase (*40*). Cheung and co-workers showed that the interaction between CaM and calcineurin at less than saturating Ca^{2+} was stimulated by decreasing pH (*84*), and suggested that pH plays a role in conformational changes in both the enzyme and CaM that contribute to activation (*41*). Many of the pH effects of enzyme activation are due to structural changes in the target, but the present results suggest that the pH-dependent activity of some enzymes may be in part due to electrostatic selection of a distinct CaM conformation that may be more or less suitable for activation. The idea of a crucial role for acidic residues in determining the CaM conformation has previously been noted by Squier and co-workers (*74*). The single-molecule results show that it is the amplitudes of distinct subconformations, and not simply a change in an average structure, that vary upon changes in solution conditions.

Nature of Multiple Substates. There are a number of possibilities for the character of the extended structure. The distance between residues 34 and 110 in the extended structure corresponds closely to the predicted distance between residues 34 and 110 in the extended Ca^{2+}-CaM crystal structures (*8*, *10*, *85*). Therefore, one possibility, consistent with the crystal structures, is that the extended structure has a helical linker separating the two opposing domains. However, this does not seem to be consistent with the increase in amplitude of the extended conformation of apoCaM-DA relative to Ca^{2+}-CaM-DA, as decreased helicity of apoCaM relative to Ca^{2+}-CaM has been observed via CD. Although it is still possible that there exists a subpopulation of apoCaM with a helical linker, a more likely possibility is that the extended conformation in apoCaM-DA is due to a partially denatured subconformation. A thermal denaturation study conducted by Privalov and co-workers observed CaM structures at different temperatures and reported a continued unfolding of the central linker at increasing temperature (*86*). On the basis of a CD study of the denaturation of CaM, Bayley and co-workers proposed that apoCaM is constantly in equilibrium between a folded and unfolded structure, with the partially unfolded conformation being more extended (*87*). Thus, it is possible that the extended conformations of apoCaM and Ca^{2+}-CaM have different structural properties. A subpopulation of apoCaM may exist with a partially unfolded central linker or C-terminal domain that leads to an increase in distance between residues 34 and 110, while the extended conformation of Ca^{2+}-CaM may be due to a helical linker, as predicted by the extended crystal structures.

CONCLUSIONS

Single-molecule FRET has revealed the presence of multiple conformations of CaM-DA in solution that are stable on the time scale of hundreds of microseconds. CaM, therefore, fits into a class of proteins where multiple, stable conformations exist to facilitate diverse function (*88*). The detection of conformational substates demonstrates the ability of single-molecule methods to characterize heterogeneity, revealing important structural features that are not readily characterized or detected by ensemble methods. In the dominant conformation, the distance between residues 34 and 110 was about 35 Å for CaM-DA and 38 Å for apoCaM-DA. An extended conformation was present around 55 Å. The distributions suggested the existence of a third conformation centered around 29 Å. A decrease in ionic strength increased the average distance between residues 34 and 110 in apoCaM-DA while increasing heterogeneity, but had little effect on Ca^{2+}-CaM-DA. The distribution in 50% ethanol showed only one broad conformation of Ca^{2+}-CaM-DA, while the change in conformation of CaM-DA upon prolonged exposure to H_2O_2 was due to an increase in amplitude of an extended conformation. The distribution of CaM-DA changed significantly toward a more compact conformation at reduced pH. The extended conformation was almost entirely absent.

We hypothesize that pH-dependent and ionic strength dependent shifts in the populations of conformational substates result from changes in electrostatic interactions in the central linker. For example, the shift in favor of the more compact conformation at reduced pH may result from the loss of electrostatic interactions that serve as electrostatic spacers at neutral pH. This hypothesis is corroborated by inspection of the proximity of side chains of glutamic acid residues and aspartic acid residues surrounding the hinge region in the compact Ca^{2+}-CaM crystal structure (*11*) (Figure 4). The pH effect on CaM structure may play a role in the interaction of CaM with targets that show a pH-dependent activation.

The presence of multiple conformations is a physical property of CaM, and it is likely that the heterogeneity of structure is at least partially responsible for the promiscuous ability of CaM to recognize diverse targets. Squier and co-workers have suggested that association of the C-terminal domain of CaM with a target may disrupt a structurally important hydrogen bond involving the central linker, facilitating formation of a compact binding conformation of CaM (*74*). The present results suggest similarly that shielding electrostatic interactions of CaM by a target may serve as a trigger for conformational changes of CaM that occur upon target recognition. In contrast, it may be that the extended conformation of CaM is necessary for the recognition of targets such as the small conductance potassium channel (*89*) or adenylate-cyclase (*90*), where CaM is in a relatively extended conformation even after target recognition and thus does not adopt the well-known compact binding conformation, while the compact structure of CaM may be more amenable to recognition of targets where a compact final structure is formed, such as CaM-dependent protein kinase II (*91*). While less diverse in its binding interactions than Ca^{2+}-CaM, apoCaM has been shown to bind to a number of enzymes, including the tetrameric ryanodine receptor (*92*, *93*) and the L-type Ca^{2+} channels (*94*), and thus the promiscuity of apoCaM binding interactions may also be aided by its structural diversity.

ACKNOWLEDGMENT

We thank Dr. Madeline Shea, Dr. Jeffrey Urbauer, and Dr. Thomas Squier for insightful discussions. We also gratefully acknowledge an anonymous reviewer for suggestions regarding measurement of free Ca^{2+} concentrations and other helpful suggestions.

REFERENCES

1. Chin, D., and Means, A. R. (2000) Calmodulin: a prototypical calcium sensor, *Trends Cell Biol. 10*, 322−328.
2. Persechini, A., and Stemmer Paul, M. (2002) Calmodulin is a limiting factor in the cell, *Trends Cardiovasc. Med. 12*, 32−37.
3. Crivici, A., and Ikura, M. (1995) Molecular and structural basis of target recognition by calmodulin, *Annu. Rev. Biophys. Biomol. Struct. 24*, 85−116.
4. Vetter, S. W., and Leclerc, E. (2003) Novel aspects of calmodulin target recognition and activation, *Eur. J. Biochem. 270*, 404−414.
5. Ikura, M., Hiraoki, T., Hikichi, K., Mikuni, T., Yazawa, M., and Yagi, K. (1983) Nuclear magnetic resonance studies on calmodulin: calcium-induced conformational change, *Biochemistry 22*, 2573−2579.
6. Williams, R. J. P. (1992) Calcium and calmodulin, *Cell Calcium 13*, 355−362.
7. VanScyoc, W. S., Sorensen, B. R., Rusinova, E., Laws, W. R., Ross, J. B. A., and Shea, M. A. (2002) Calcium binding to calmodulin mutants monitored by domain-specific intrinsic phenylalanine and tyrosine fluorescence, *Biophys. J. 83*, 2767−2780.
8. Chattopadhyaya, R., Meador, W. E., Means, A. R., and Quiocho, F. A. (1992) Calmodulin structure refined at 1.7 Å resolution, *J. Mol. Biol. 228*, 1177−1192.
9. Slaughter, B. D., Allen, M. W., Unruh, J. R., Urbauer, R. J. B., and Johnson, C. K. (2004) Single-molecule resonance energy transfer and fluorescence correlation spectroscopy of calmodulin in solution, *J. Phys. Chem. B 108*, 10388−10397.
10. Wilson, M. A., and Brunger, A. T. (2000) The 1.0 Å crystal structure of calcium-bound calmodulin: an analysis of disorder and implications for functionally relevant plasticity, *J. Mol. Biol. 301*, 1237−1256.
11. Fallon, J. L., and Quiocho, F. A. (2003) A closed compact structure of native calcium-calmodulin, *Structure 11*, 1303−1307.
12. Kuboniwa, H., Tjandra, N., Grzesiek, S., Ren, H., Klee, C. B., and Bax, A. (1995) Solution structure of calcium-free calmodulin, *Nat. Struct. Biol. 2*, 768−776.
13. Zhang, M., Tanaka, T., and Ikura, M. (1995) Calcium-induced conformational transition revealed by the solution structure of apo calmodulin, *Nat. Struct. Biol. 2*, 758−767.
14. Barbato, G., Ikura, M., Kay, L. E., Pastor, R. W., and Bax, A. (1992) Backbone dynamics of calmodulin studied by 15N relaxation using inverse detected two-dimensional NMR spectroscopy: the central helix is flexible, *Biochemistry 31*, 5269−5278.
15. Yamniuk, A. P., and Vogel, H. J. (2004) Calmodulin's flexibility allows for promiscuity in its interactions with target proteins and peptides, *Mol. Biotechnol. 27*, 33−58.
16. Babu, Y. S., Sack, J. S., Greenhough, T. J., Bugg, C. E., Means, A. R., and Cook, W. J. (1985) Three-dimensional structure of calmodulin, *Nature 315*, 37−40.
17. Baber, J. L., Szabo, A., and Tjandra, N. (2001) Analysis of slow interdomain motion of macromolecules using NMR relaxation data, *J. Am. Chem. Soc. 123*, 3953−3959.
18. Bertini, I., Del Bianco, C., Gelis, I., Katsaros, N., Luchinat, C., Parigi, G., Peana, M., Provenzani, A., and Zoroddu, M. A. (2004) Experimentally exploring the conformational space sampled by domain reorientation in calmodulin, *Proc. Natl. Acad. Sci. U.S.A. 101*, 6841−6846.
19. Chang, S.-L., Szabo, A., and Tjandra, N. (2003) Temperature dependence of domain motions of calmodulin probed by NMR relaxation at multiple fields, *J. Am. Chem. Soc. 125*, 11379−11384.
20. Wriggers, W., Mehler, E., Pitici, F., Weinstein, H., and Schulten, K. (1998) Structure and dynamics of calmodulin in solution, *Biophys. J. 74*, 1622−1639.
21. Yang, C., Jas, G. S., and Kuczera, K. (2001) Structure and dynamics of calcium-activated calmodulin in solution, *J. Biomol. Struct. Dyn. 19*, 247−271.
22. Török, K., Tzortzopoulos, A., Grabarek, Z., Best, S. L., and Thorogate, R. (2001) Dual effect of ATP in the activation mechanism of brain Ca^{2+}/calmodulin-dependent protein kinase II by Ca^{2+}/calmodulin, *Biochemistry 40*, 14878−14890.
23. Yao, Y., Schoeneich, C., and Squier, T. C. (1994) Resolution of structural changes associated with calcium activation of calmodulin using frequency domain fluorescence spectroscopy, *Biochemistry 33*, 7797−7810.
24. Vogel, H. J., Brokx, R. D., and Ouyang, H. (2002) Calcium-binding proteins, *Methods Mol. Biol. 172*, 3−20.
25. Urbauer, J. L., Short, J. H., Dow, L. K., and Wand, A. J. (1995) Structural analysis of a novel interaction by calmodulin: high-affinity binding of a peptide in the absence of calcium, *Biochemistry 34*, 8099−8109.
26. Tjandra, N., Kuboniwa, H., Ren, H., and Bax, A. (1995) Rotational dynamics of calcium-free calmodulin studied by 15N-NMR relaxation measurements, *Eur. J. Biochem. 230*, 1014−24.
27. Moerner, W. E., and Orrit, M. (1999) Illuminating single molecules in condensed matter, *Science 283*, 1670−1676.
28. Weiss, S. (2000) Measuring conformational dynamics of biomolecules by single molecule fluorescence spectroscopy, *Nat. Struct. Biol. 7*, 724−729.
29. Xie, X. S., and Trautman, J. K. (1998) Optical studies of single molecules at room temperature, *Annu. Rev. Phys. Chem. 49*, 441−480.
30. Deniz, A. A., Dahan, M., Grunwell, J. R., Ha, T., Faulhaber, A. E., Chemla, D. S., Weiss, S., and Schultz, P. G. (1999) Single-pair fluorescence resonance energy transfer on freely diffusing molecules: observation of Forster distance dependence and subpopulations, *Proc. Natl. Acad. Sci. U.S.A. 96*, 3670−3675.
31. Ha, T., Ting, A. Y., Liang, J., Caldwell, W. B., Deniz, A. A., Chemla, D. S., Schultz, P. G., and Weiss, S. (1999) Single-molecule fluorescence spectroscopy of enzyme conformational dynamics and cleavage mechanism, *Proc. Natl. Acad. Sci. U.S.A. 96*, 893−898.
32. Ha, T. (2004) Structural dynamics and processing of nucleic acids revealed by single-molecule spectroscopy, *Biochemistry 43*, 4055−4063.
33. Talaga, D. S., Lau, W. L., Roder, H., Tang, J., Jia, Y., DeGrado, W. F., and Hochstrasser, R. M. (2000) Dynamics and folding of single two-stranded coiled-coil peptides studied by fluorescent energy transfer confocal microscopy, *Proc. Natl. Acad. Sci. U.S.A. 97*, 13021−13026.
34. Brasselet, S., Peterman, E. J. G., Miyawaki, A., and Moerner, W. E. (2000) Single-molecule fluorescence resonant energy transfer in calcium concentration dependent cameleon, *J. Phys. Chem. B 104*, 3676−3682.
35. Tan, X., Hu, D., Squier, T. C., and Lu, H. P. (2004) Probing nanosecond protein motions of calmodulin by single-molecule fluorescence anisotropy, *Appl. Phys. Lett. 85*, 2420−2422.
36. Tang, J., Mei, E., Green, C., Kaplan, J., DeGrado, W. F., Smith, A. B., III, and Hochstrasser, R. M. (2004) Probing structural dynamics of individual calmodulin:peptide complexes in hydrogels by single-molecule confocal microscopy, *J. Phys. Chem. B 108*, 15910−15918.
37. Allen, M. W., Bieber Urbauer, R. J., and Johnson, C. K. (2004) Single-molecule assays of calmodulin target binding detected with a calmodulin energy-transfer construct, *Anal. Chem. 76*, 3630−3637.
38. Allen, M. W., Urbauer, R. J. B., Zaidi, A., Williams, T. D., Urbauer, J. L., and Johnson, C. K. (2004) Fluorescence labeling, purification and immobilization of a double cysteine mutant calmodulin fusion protein for single-molecule experiments, *Anal. Biochem. 325*, 273−284.
39. Milos, M., Schaer, J. J., Comte, M., and Cox, J. A. (1988) Microcalorimetric investigation of the interaction of calmodulin with seminalplasmin and myosin light chain kinase, *J. Biol. Chem. 263*, 9218−9222.
40. Kee, S. M., and Graves, D. J. (1987) Properties of the G subunit of phosphorylase kinase, *J. Biol. Chem. 262*, 9448−9453.
41. Huang, S., Carlson, G. M., and Cheung, W. Y. (1994) Calmodulin-dependent enzymes undergo a proton-induced conformational change that is associated with their interactions with calmodulin, *J. Biol. Chem. 269*, 7631−7638.
42. Gao, J., Yin, D., Yao, Y., Williams, T. D., and Squier, T. C. (1998) Progressive decline in the ability of calmodulin isolated from aged

brain to activate the plasma membrane calcium-ATPase, *Biochemistry 37*, 9536−9548.
43. Yao, Y., Yin, D., Jas, G., Kuczera, K., Williams, T. D., Schoeneich, C., and Squier, T. C. (1996) Oxidative modification of a carboxyl-terminal vicinal methionine in calmodulin by hydrogen peroxide inhibits calmodulin-dependent activation of the plasma membrane calcium-ATPase, *Biochemistry 35*, 2767−2787.
44. Grimaud, R., Ezraty, B., Mitchell, J. K., Lafitte, D., Briand, C., Derrick, P. J., and Barras, F. (2001) Repair of oxidized proteins: identification of a new methionine sulfoxide reductase, *J. Biol. Chem. 276*, 48915−48920.
45. Sun, H., Gao, J., Ferrington, D. A., Biesiada, H., Williams, T. D., and Squier, T. C. (1999) Repair of oxidized calmodulin by methionine sulfoxide reductase restores ability to activate the plasma membrane Ca-ATPase, *Biochemistry 38*, 105−112.
46. Squier, T. C., and Bigelow, D. J. (2000) Protein oxidation and age-dependent alterations in calcium homeostasis, *Front. Biosci. 5*, d504−526.
47. Allen, M. W. Analytical chemistry at the extremes: Ultrafast and single-molecule fluorescence spectroscopic investigations of biological systems. Ph.D. Dissertation, University of Kansas, Lawrence, KS, 2004.
48. Weiner, M. P., Costa, G. L., Schoettlin, W., Cline, J., Mathur, E., and Bauer, J. C. (1994) Site-directed mutagenesis of double-stranded DNA by the polymerase chain reaction, *Gene 151*, 119−123.
49. Hemsley, A., Arnheim, N., Toney, M. D., Cortopassi, G., and Galas, D. J. (1989) A simple method for site-directed mutagenesis using the polymerase chain reaction, *Nucleic Acids Res. 17*, 6545−6551.
50. Osborn, K. D., Zaidi, A., Mandal, A., Urbauer, R. J. B., and Johnson, C. K. (2004) Single-molecule dynamics of the calcium-dependent activation of plasma-membrane Ca^{2+}-ATPase by calmodulin, *Biophys. J. 87*, 1892−1899.
51. Bartlett, R. K., Bieber Urbauer, R. J., Anbanandam, A., Smallwood, H. S., Urbauer, J. L., and Squier, T. C. (2003) Oxidation of Met144 and Met145 in calmodulin blocks calmodulin dependent activation of the plasma membrane Ca-ATPase, *Biochemistry 42*, 3231−3238.
52. Dahan, M., Deniz, A. A., Ha, T., Chemla, D. S., Schultz, P. G., and Weiss, S. (1999) Ratiometric measurement and identification of single diffusing molecules, *Chem. Phys. 247*, 85−106.
53. Schuler, B., Lipman, E. A., and Eaton, W. A. (2002) Probing the free-energy surface for protein folding with single-molecule fluorescence spectroscopy, *Nature 419*, 743−747.
54. Grunwell, J. R., Glass, J. L., Lacoste, T. D., Deniz, A. A., Chemla, D. S., and Schultz, P. G. (2001) Monitoring the conformational fluctuations of DNA hairpins using single-pair fluorescence resonance energy transfer, *J. Am. Chem. Soc. 123*, 4295−4303.
55. Van der Meer, B. W., Coker, G., and Chen, S.-Y. (1994) *Resonance energy transfer: theory and data*, VCH, New York.
56. Harms, G. S., Pauls, S. W., Hedstrom, J. F., and Johnson, C. K. (1997) Tyrosyl fluorescence decays and rotational dynamics in tyrosine monomers and in dipeptides, *J. Fluoresc. 7*, 273−281.
57. Lakowicz, J. R. (1999) *Principles of Fluorescence Spectroscopy*, 2nd ed., Kluwer Academic/Plenum, New York.
58. Johnson, M. L., and Faunt, L. M. (1992) Parameter estimation by least-squares methods, *Methods Enzymol. 210*, 1−37.
59. Sorensen, B. R., and Shea, M. A. (1998) Interactions between domains of apo calmodulin alter calcium binding and stability, *Biochemistry 37*, 4244−4253.
60. VanScyoc, W. S., and Shea, M. A. (2001) Phenylalanine fluorescence studies of calcium binding to N-domain fragments of *Paramecium* calmodulin mutants show increased calcium affinity correlates with increased disorder, *Protein Sci. 10*, 1758−1768.
61. Sorensen, B. R., Faga, L. A., Hultman, R., and Shea, M. A. (2002) An interdomain linker increases the thermostability and decreases the calcium affinity of the calmodulin N-domain, *Biochemistry 41*, 15−20.
62. Pedigo, S., and Shea, M. A. (1995) Quantitative endoproteinase GluC footprinting of cooperative calcium binding to calmodulin: proteolytic susceptibility of E31 and E87 indicates interdomain interactions, *Biochemistry 34*, 1179−1196.
63. Brokx, R. D., Scheek, R. M., Weljie, A. M., and Vogel, H. J. (2004) Backbone dynamic properties of the central linker region of calcium-calmodulin in 35% trifluoroethanol, *J. Struct. Biol. 146*, 272−280.
64. Bayley, P. M., and Martin, S. R. (1992) The α-helical content of calmodulin in increased by solution conditions favouring protein crystallisation, *Biochim. Biophys. Acta 1160*, 16−21.
65. Ha, T. (2001) Single-molecule fluorescence resonance energy transfer, *Methods 25*, 78−86.
66. Van der Meer, B. W. (2002) Kappa-squared: from nuisance to new sense, *Rev. Mol. Biotechnol. 82*, 181−196.
67. Haas, E., Katchalski-Katzir, E., and Steinberg, I. Z. (1978) Effect of the orientation of donor and acceptor on the probability of energy transfer involving electronic transitions of mixed polarization, *Biochemistry 17*, 5064−5070.
68. Linse, S., Helmersson, A., and Forsen, S. (1991) Calcium binding to calmodulin and its globular domains, *J. Biol. Chem. 266*, 8050−8054.
69. Jaren, O. R., Harmon, S., Chen, A. F., and Shea, M. A. (2000) *Paramecium* calmodulin mutants defective in ion channel regulation can bind calcium and undergo calcium-induced conformational switching, *Biochemistry 39*, 6881−6890.
70. Pedigo, S., and Shea, M. A. (1995) Quantitative endoproteinase GluC footprinting of cooperative Ca^{2+} binding to calmodulin: proteolytic susceptibility of E31 and E87 indicates interdomain interactions, *Biochemistry 34*, 1179−1196.
71. Sorensen, B. R., and Shea Madeline, A. (1996) Calcium binding decreases the Stokes radius of calmodulin and mutants R74A, R90A, and R90G, *Biophys. J. 71*, 3407−3420.
72. Jaren, O. R., Kranz, J. K., Sorensen, B. R., Wand, A. J., and Shea, M. A. (2002) Calcium-induced conformational switching of Paramecium calmodulin provides evidence for domain coupling, *Biochemistry 41*, 14158−14166.
73. Bayley, P. M., Findlay, W. A., and Martin, S. R. (1996) Target recognition by calmodulin: dissecting the kinetics and affinity of interaction using short peptide sequences, *Protein Sci. 5*, 1215−1228.
74. Sun, H., Yin, D., and Squier, T. C. (1999) Calcium-dependent structural coupling between opposing globular domains of calmodulin involves the central helix, *Biochemistry 38*, 12266−12279.
75. Kuhlman, B., Luisi, D. L., Young, P., and Raleigh, D. P. (1999) pK_a values and the pH dependent stability of the N-terminal domain of L9 as probes of electrostatic interactions in the denatured state. Differentiation between local and nonlocal interactions, *Biochemistry 38*, 4896−4903.
76. Merz, K. M., Jr. (1991) Determination of pK_as of ionizable groups in proteins: the pK_a of Glu 7 and 35 in hen eggs white lysozyme and Glu 106 in human carbonic anhydrase II, *J. Am. Chem. Soc. 113*, 3572−3575.
77. Protasevich, I., Ranjbar, B., Lobachov, V., Makarov, A., Gilli, R., Briand, C., Lafitte, D., and Haiech, J. (1997) Conformation and thermal denaturation of apocalmodulin: role of electrostatic mutations, *Biochemistry 36*, 2017−2024.
78. Meador, W. E., Means, A. R., and Quiocho, F. A. (1993) Modulation of calmodulin plasticity in molecular recognition on the basis of x-ray structures, *Science 262*, 1718−1721.
79. Gao, J., Yao, Y., and Squier, T. C. (2001) Oxidatively modified calmodulin binds to the plasma membrane calcium-ATPase in a nonproductive and conformationally disordered complex, *Biophys. J. 80*, 1791−1801.
80. Osborn, K. D., Bartlett, R. K., Mandal, A., Zaidi, A., Urbauer, R. J. B., Urbauer, J. L., Galeva, N., Williams, T. D., and Johnson, C. K. (2004) Single-molecule dynamics reveal an altered conformation for the autoinhibitory domain of plasma membrane Ca2+-ATPase bound to oxidatively modified calmodulin, *Biochemistry 43*, 12937−12944.
81. Chin, D., and Means, A. R. (1996) Methionine to glutamine substitutions in the C-terminal domain of calmodulin impair the activation of three protein kinases, *J. Biol. Chem. 271*, 30465−30471.
82. Blumenthal, D. K., and Stull, J. T. (1982) Effects of pH, ionic strength, and temperature on activation by calmodulin and catalytic activity of myosin light-chain kinase, *Biochemistry 21*, 2386−2391.
83. Tkachuk, V. A., and Men'shikov, M. Y. (1981) Effect of pH on calcium-binding properties of calmodulin and on its interaction with calcium-dependent cyclic nucleotide phosphodiesterase, *Biokhimiya (Moscow) 46*, 963−973.
84. Huang, S., and Cheung, W. Y. (1994) H^+ is involved in the activation of calcineurin by calmodulin, *J. Biol. Chem. 269*, 22067−22074.

85. Babu, Y. S., Bugg, C. E., and Cook, W. J. (1988) Structure of calmodulin refined at 2.2 Å resolution, *J. Mol. Biol. 204*, 191−204.
86. Wintrode, P. L., and Privalov, P. L. (1997) Energetics of target peptide recognition by calmodulin: a calorimetric study, *J. Mol. Biol. 266*, 1050−1062.
87. Masino, L., Martin, S. R., and Bayley, P. M. (2000) Ligand binding and thermodynamic stability of a multidomain protein, calmodulin, *Protein Sci. 9*, 1519−1529.
88. James, L. C., and Tawfik, D. S. (2003) Conformational diversity and protein evolution—a 60-year-old hypothesis revisited, *Trends Biochem. Sci. 28*, 361−368.
89. Schumacher, M. A., Rivard, A. F., Bichinger, H. P., and Adelman, J. P. (2001) Structure of the gating domain of a calcium-activated potassium channel complexed with calcium-calmodulin, *Nature 410*, 1120−1124.
90. Drum, C. L., Yan, S.-Z., Bardt, J., Shen, Y.-Q., Lu, D., Soelalman, S., Grabarek, Z., Bohnm, A., and Tang, W.-J. (2002) Structural basis for the activation of anthrax adenylyl cyclase exotoxin by calmodulin, *Nature 415*, 396−402.
91. Meador, W. E., Means, A. R., and Quiocho, F. A. (1992) Target enzyme recognition by calmodulin: 2.4 Å structure of a calmodulin-peptide complex, *Science 257*, 1251−1255.
92. Moore, C. P., Rodney, G., Zhang, J.-Z., Santacruz-Toloza, L., Strasburg, G., and Hamilton, S. L. (1999) Apocalmodulin and calcium-calmodulin bind to the same region on the skeletal muscle calcium release channel, *Biochemistry 38*, 8532−8537.
93. Xiong, L.-W., Newman, R. A., Rodney, G. G., Thomas, O., Zhang, J.-Z., Persechini, A., Shea, M. A., and Hamilton, S. L. (2002) Lobe-dependent regulation of ryanodine receptor type 1 by calmodulin, *J. Biol. Chem. 277*, 40862−40870.
94. Ehlers, M. D., and Augustine, G. J. (1999) Cell signalling. Calmodulin at the channel gate, *Nature 399*, 107−108.

BI048595O